Computers and Fluids 158 (2017) 167–175

Contents lists available at ScienceDirect

Computers and Fluids

journal homepage: www.elsevier.com/locate/compfluid

Benchmark solutions

FSI Simulation of two back-to-back wind turbines in atmospheric boundary layer flow

A. Korobenko[a], J. Yan[b], S.M.I. Gohari[c], S. Sarkar[c], Y. Bazilevs[b,*]

[a] Department of Mechanical and Manufacturing Engineering, University of Calgary, Calgary, AB T2N 1N4, Canada
[b] Department of Structural Engineering, University of California, San Diego, La Jolla, CA 92093, USA
[c] Department of Mechanical and Aerospace Engineering, University of California, San Diego, La Jolla, CA 92093, USA

ARTICLE INFO

Article history:
Received 15 September 2016
Revised 20 April 2017
Accepted 12 May 2017
Available online 19 May 2017

Keywords:
Stably-stratified ABL
ALE-VMS
FSI
Multi-domain method
Wake-turbine interaction
IGA

ABSTRACT

The paper presents aerodynamic and fluid–structure interaction (FSI) simulations of two back-to-back 5 MW horizontal-axis wind turbines (HAWTs) at full scale and with full geometrical complexity operating in a stably-stratified atmospheric boundary layer (ABL) flow. The numerical formulation for stratified incompressible flows is based on the ALE-VMS methodology, and is coupled to a Kirchhoff–Love thin-shell formulation employed to model the wind-turbine structure. A multi-domain method (MDM) is adopted for computational efficiency. In the simulations presented the wind turbines are positioned one behind the other at a distance of four rotor diameters, which results in a noticeable power production loss for the downstream turbine due to the wake velocity deficit of the upstream turbine. The importance of including FSI coupling in the modeling to better predict the unsteady aerodynamic loads acting on the wind-turbine blades is also highlighted.

1. Introduction

Wind turbines arranged in arrays operate in complex turbulent atmospheric boundary layer (ABL) flows with a wide range of energy-containing scales, and in different atmospheric stability regimes. Wind turbines positioned downstream operate in the wakes generated by upstream turbines, and have been observed to generate less power compared to the upstream turbines. In addition, downstream turbines experience higher variations in aerodynamic loads, which tend to shorten their fatigue life. Depending on the atmospheric stability regime, spacing between turbines, the underlying surface topology, turbulence intensity, and wind direction and speed, the power-generation deficit for the downstream turbines may be as high as 40%, as was reported in [1,2].

To better understand the conditions under which such power production losses occur, and to get a better estimate of the unsteady aerodynamic loading causing premature turbine failure, it is important to have good wind-turbine-farm-level measurement data as well as advanced, validated modeling methodologies and tools for these systems. In addition, the ability to dynamically integrate simulations and measurements into a single predictive modeling framework [3] may lead to further advances in wind-energy technology.

As the wind energy sector continues to grow, more wind turbines are designed and built to operate in mountainous regions and in offshore environments, where the background stratification has significant effects on wind-turbine performance. As a result, in recent years, several experimental and numerical studies have been carried out to better understand wind-power generation in ABL flows. Effects of atmospheric stability on wind-turbine power production were studied through the analysis of data collected in actual wind farms in [1,2,4]. Influence of atmospheric stability conditions on power production were also studied in [5] using measurements in a stratified-flow wind tunnel, and in [6] through field-test measurements of a single wake. A cooled ABL has a shallow inversion layer which can exceed the blade tip maximum height and turbulence properties that are quite different when compared to convective and neutral regimes. The numerical approach developed here provides a way forward to include realistic ABL computational data in wind turbine simulations.

A common approach to numerically simulate wind turbines in ABL flows is to use large-eddy simulations (LES) in combination with actuator-line models, which represent the effect of wind turbines in the flow. A study of near-wake structures of a single turbine in a stably stratified ABL was performed in [7,8]. The effect of the Coriolis force on the turbine wake structure was studied in [9]. The above mentioned studies focused on aerodynamics only,

* Corresponding author.
E-mail addresses: yuri@ucsd.edu, jbazilevs@ucsd.edu (Y. Bazilevs).

http://dx.doi.org/10.1016/j.compfluid.2017.05.010
0045-7930/

without considering structural coupling and complex geometry of the wind-turbine components. An attempt to investigate structural response of wind turbines in ABL and the remaining fatigue-life in downwind turbines was made in [10] using an LES solver coupled to low-fidelity aerodynamics and structural mechanics wind-turbine models [11]. The effect of atmospheric stability on the blade-root moment and low-speed shaft torque was studied in [12], but also without considering the full complexity of the blade geometry and material distribution.

The current paper focuses on methods developed for modeling of multi-megawatt wind turbines at full-scale operating in realistic stably-stratified ABL flows. Full complexity of aerodynamics, structural mechanics, and wind-turbine geometry is considered in the modeling approaches presented in this paper. The methods presented herein form a foundation for predictive FSI modeling for multiple wind turbines operating in ABL flows. To the best of our knowledge FSI simulations of multiple turbines are reported in open literature for the first time.

The paper is organized as follows. In Section 2, we present the governing equations for aerodynamics of ABL flow, structural mechanics, and their coupling. Discretization techniques for the FSI formulation employed are discussed in Section 3. In Section 4, we describe how we employ the Multi-Domain Method (MDM) [13–17] in the modeling of wind-turbine FSI, report the results of aerodynamics and FSI simulations of two back-to-back 5 MW horizontal-axis wind turbines (HAWTs) operating in a stably-stratified ABL, and compare the aerodynamic performance of the upstream and downstream turbines. In Section 5, we draw conclusions.

2. Governing equations

The aerodynamics of wind turbines in ABL flows is governed by the Navier–Stokes equations of incompressible flows with the Boussinesq approximation. The equations are posed on a moving domain using the Arbitrary Lagrangian–Eulerian (ALE) description [18], and are written as

$$\rho_1\left(\left.\frac{\partial \mathbf{u}}{\partial t}\right|_{\hat{x}} + (\mathbf{u}-\hat{\mathbf{u}})\cdot\nabla\mathbf{u} - \mathbf{f}_1\right) - \nabla\cdot\boldsymbol{\sigma}_1 - \mathbf{f}_b = \mathbf{0}, \tag{1}$$

$$\nabla\cdot\mathbf{u} = 0, \tag{2}$$

where ρ_1 is the fluid density, $\mathbf{u}$ is the fluid velocity, $\hat{\mathbf{u}}$ is the velocity of the fluid domain, $\mathbf{f}_1$ is the fluid body force per unit mass, $\mathbf{f}_b$ is Boussinesq forcing term, and $\boldsymbol{\sigma}_1$ is the fluid Cauchy stress defined as

$$\boldsymbol{\sigma}_1(\mathbf{u}, p) = -p\mathbf{I} + 2\mu\nabla^s\mathbf{u}, \tag{3}$$

where $\mathbf{I}$ is the identity tensor, p is the pressure, μ is the dynamic viscosity, and ∇^s is the symmetric gradient operator.

To model the temperature distribution in a thermally-stratified ABL, a time-dependent scalar advection-diffusion equation is employed,

$$\left.\frac{\partial \phi}{\partial t}\right|_{\hat{x}} + (\mathbf{u}-\hat{\mathbf{u}})\cdot\nabla\phi - \nabla\cdot\nu_\phi\nabla\phi = 0, \tag{4}$$

where ν_ϕ is the diffusivity, and ϕ is the potential temperature, which is decomposed into two parts, namely,

$$\phi(\mathbf{x}, t) = \bar{\phi}(x_3) + \phi'(\mathbf{x}, t), \tag{5}$$

where $\bar{\phi}(x_3)$ is the background temperature field varying in the direction of gravity and ϕ' is a temporally and spatially varying temperature fluctuation. The temperature field ϕ enters the Navier–Stokes momentum equations through the Boussinesq forcing term $\mathbf{f}_b$, which is given by

$$\mathbf{f}_b = \rho_1\, g\frac{\phi'}{\phi_0}\mathbf{e}_3 \tag{6}$$

where ϕ_0 is the reference temperature assumed constant in the Boussinesq approximation, g is the gravitational acceleration magnitude, and $\mathbf{e}_3$ is the Cartesian basis vector pointing in the direction of gravity.

To arrive at this form of the Boussinesq forcing term, we first consider the equation of state

$$pM = \rho R\phi, \tag{7}$$

where M and R are the molar mass and universal gas constant, respectively. According to the Boussinesq approximation, density variation $\Delta\rho$ only appears in the term of the momentum equation that is multiplied by the gravity vector, i.e., $f_b = \Delta\rho\cdot g\mathbf{e}_3$ (this term is also called the buoyancy force, which only acts in the direction of gravity). In all other terms density is assumed to be constant and equal ρ_1. Density variation is assumed to only depend on temperature variation. As a result, the relative change in density may be expressed as

$$\frac{\Delta\rho}{\rho_1} = -\alpha\cdot\phi', \tag{8}$$

where α is the coefficient of thermal expansion, which, for an ideal gas, is given by

$$\alpha = \frac{1}{\phi_0}. \tag{9}$$

The minus sign in Eq. (8) ensures that increase in temperature leads to decrease in density.

To model Earth's rotation, the Coriolis forcing term is added to Eq. (1), and is given by

$$\mathbf{f}_{1i} = f_c\epsilon_{ij3}u_j\mathbf{e}_i \tag{10}$$

where f_c is the Coriolis parameter and ϵ_{ijk} are the Cartesian components of the alternator tensor.

Remark. In Eqs. (1) and (4), the time derivatives are taken holding the referential-domain coordinates $\hat{\mathbf{x}}$ fixed, while the space derivatives are taken with respect to the spatial coordinates of the current configuration $\mathbf{x}$.

The governing equations of structural mechanics, written in the Lagrangian frame [19], consist of the local balance of linear momentum, and are given by

$$\rho_2\left(\frac{\mathrm{d}^2\mathbf{y}}{\mathrm{d}t^2} - \boldsymbol{f}_2\right) - \nabla\cdot\boldsymbol{\sigma}_2 = \mathbf{0} \tag{11}$$

where ρ_2 is the structure density, $\boldsymbol{f}_2$ is the structure body force per unit mass, $\boldsymbol{\sigma}_2$ is the structure Cauchy stress, $\mathbf{y}$ is the structure displacement vector, and the time derivatives are taken holding the material coordinates fixed.

At the fluid-structure interface, compatibility of the kinematics and tractions is enforced, namely,

$$\mathbf{u} - \frac{\mathrm{d}\mathbf{y}}{\mathrm{d}t} = \mathbf{0}, \tag{12}$$

$$\boldsymbol{\sigma}_1\mathbf{n}_1 + \boldsymbol{\sigma}_2\mathbf{n}_2 = \mathbf{0}, \tag{13}$$

where $\mathbf{n}_1$ and $\mathbf{n}_2$ are the unit outward normal vectors to the fluid and structural mechanics domains, respectively.

In the following, a discretization of the above formulation applicable to the FSI modeling of wind turbines in ABL flows is discussed. A comprehensive discussion of discretization options, coupling strategies, and other aspects of computational FSI may be found in a recent book [20].

3. Discretization methods and FSI solution strategy

The aerodynamics formulation for stratified incompressible flows is based on the Arbitrary Lagrangian–Eulerian Variational Multiscale (ALE-VMS) method [21–26] and weak enforcement of essential boundary conditions [27–32]. The former may be viewed as an extension of the residual-based variational multi-scale (RBVMS) LES turbulence model [33,34] to moving domains using the ALE technique, while the latter acts as a near-wall model and relaxes the boundary-layer resolution requirements for engineering applications without significant loss of solution accuracy. VMS methods, in context of both ALE and space–time techniques, have been successfully applied to a wide range of engineering problems [17,24,25,32,35–56]. The stratified-flow ALE-VMS formulation is discretized in the present work using linear finite elements.

Remark. The stratified-flow ALE-VMS formulation employed in the present work is taken from a recent paper [26], where the velocity, pressure, and temperature fine scales were assumed to be proportional to the strong residuals of their respective equations. Improved VMS formulations where the coupling between the Navier-Stokes momentum and temperature equations is taken into account in the construction of the fine scales were presented in [17] and [57]. For the background, as well as more recent publications on stabilized and multiscale methods in fluid mechanics the reader is referred to [17,42,57–62].

To perform the FSI simulations of the full wind turbine configuration and capture the interaction between the rotor and tower, following [63], the fluid domain is divided into subdomain R and subdomain S. Subdomain R encloses the entire wind turbine rotor and rotates with it, while the subdomain S is a stationary domain which encloses the rest of the turbine. The interior of the rotating subdomain R is allowed to deform to accommodate the motion of the wind-turbine blades. However, the motion of the outer boundary of the subdomain R is restricted to a rigid rotation to maintain geometric compatibility with the stationary subdomain S. As the wind turbine rotor rotates, a sliding interface is created between the two subdomains. The compatibility conditions enforced at the sliding interface are

$$\mathbf{u}_R - \mathbf{u}_S = \mathbf{0}, \tag{14}$$

$$\left(-p_R\mathbf{I} + 2\mu\nabla^s\mathbf{u}_R\right)\mathbf{n}_R + \left(-p_S\mathbf{I} + 2\mu\nabla^s\mathbf{u}_S\right)\mathbf{n}_S = \mathbf{0}, \tag{15}$$

$$\phi_R - \phi_S = 0, \tag{16}$$

$$\nu_\phi\nabla\phi_R\cdot\mathbf{n}_R + \nu_\phi\nabla\phi_S\cdot\mathbf{n}_S = 0, \tag{17}$$

where all quantities with subscripts R and S refer to rotating and stationary subdomain, respectively, and $\mathbf{n}_R$ and $\mathbf{n}_S$ are the corresponding unit outward normal vectors. Compatibility conditions given by Eqs. (14)–(17) are enforced weakly through the framework of the sliding-interface methods [20,31,64], which are now widely used to handle flows about objects in relative motion in many engineering applications [35,37,65,66], including problems with non-stationary sliding interfaces [67,68].

Structural mechanics modeling of wind turbines makes use of rotation-free Kirchhoff–Love shells [69–71] discretized using Isogeometric Analysis (IGA) based on non-uniform rational B-splines (NURBS) [72,73]. Using Kirchhoff–Love shells for structural modeling presents a good combination of efficiency (since only displacement degrees-of freedom are employed in the formulation), accuracy (since NURBS are a higher-order accurate discretization technique [74]), and robustness. The latter refers to the fact that higher-order continuity of NURBS induces smooth deformation of the structural surface, which in turn, leads to a smooth deformation of the fluid mechanics mesh at the fluid-structure interface, and results in better quality of boundary-layer discretization near moving structural surfaces.

The coupled FSI problem is formulated using an augmented Lagrangian approach originally proposed in [75] for non-matching fluid–structure interface discretizations. The key feature of the method is a formal elimination of the Lagrange multiplier variable, which results in a weak enforcement of the interface compatibility conditions using only primal variables (i.e., fluid velocity and pressure, structure displacement, and temperature), and, consequently, leads to increased efficiency compared to classical Lagrange multiplier methods.

Generalized-α method [76–78] is employed to advance the FSI equations in time. In all simulations the high-frequency dissipation parameter of the Generalized-α method is set to $\rho_\infty = 0.5$. A simple block-iterative FSI solution strategy [20,61,79–81] is employed to solve the discrete FSI equations at each nonlinear iteration within a time step. The block iterative approach is a strongly coupled FSI technique where, at the level of nonlinear iterations, increments of the fluid (including fluid velocity, pressure and temperature), structure, and mesh discrete unknowns are computed sequentially. Block-iterative coupling is found to be the most efficient solution strategy for wind-turbine FSI simulations.

Remark. The fluid mesh motion is handled by solving the equations of elastostatics with Jacobian-based stiffening [61,79,82–84] to better preserve the mesh quality.

Remark. An alternative method to deal with objects in relative motion, in the space-time (ST) context, is the ST/NURBS Mesh Update Method, called "STNMUM" [42–45,85–87]. This method was applied in the references cited to flapping-wing aerodynamics and FSI and wind-turbine aerodynamics. It is more general and easier to use than the Shear-Slip Mesh Update Method (SSMUM) [88–90]. The ST Slip Interface (ST-SI) method [31], which is essentially the ST version of the sliding interface method, is even easier to use and has been applied to a number of challenging problems [31,32,91–95]. Quite often, the ST-SI method is used together with other ST methods, such as the ST Topology Change (ST-TC) method [96] and the ST method with continuous representation in time (ST-C) [97].

4. Two back-to-back wind turbines in ABL flow

We consider two back-to-back NREL 5 MW HAWTs [98] operating in ABL flow. This turbine design was previously simulated under uniform flow conditions in [42,63,68,70,75,99–101], and in stably-stratified ABL in [26], although a rotor-only aerodynamics computation was performed in the latter reference.

Each turbine has a rotor that is 120 m in diameter mounted on an 80 m tower and operating at constant, fixed rotor speed of 9 rpm. This rotor speed gives the optimal tip-speed ratio for 8 m/s wind [98], which is also the geostrophic wind speed used in the present computations.

4.1. Computational setup and boundary conditions

Two wind turbines are positioned one behind the other at a distance of 480 m, which corresponds to four rotor diameters. As a result, the wake generated by the upstream turbine needs to be accurately computed over a long domain before it impacts the downstream turbine, which poses a significant computational challenge due to a very large problem size. To circumvent this difficulty, a multi-domain method (MDM), originally proposed in [102], is adopted in the present work to efficiently separate the two turbine domains. We note that the MDM was successfully applied to a number of challenging 3D problems, including flow around a small wing placed in the wake of a larger wing [102], flow in the wake of

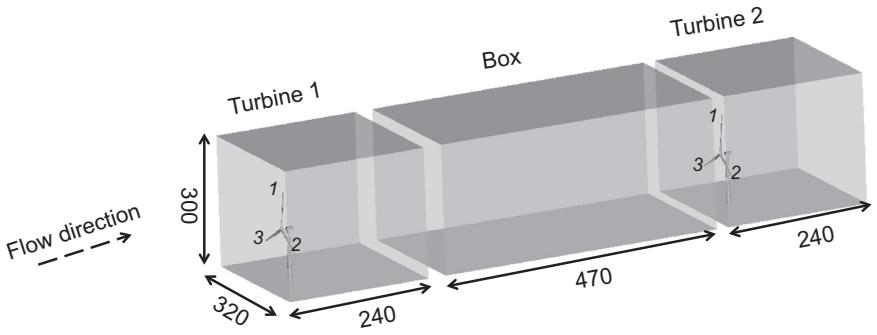

Fig. 1. Problem setup for the multi-domain wind-turbine simulation. The subdomains are labeled and all the dimensions are in m.

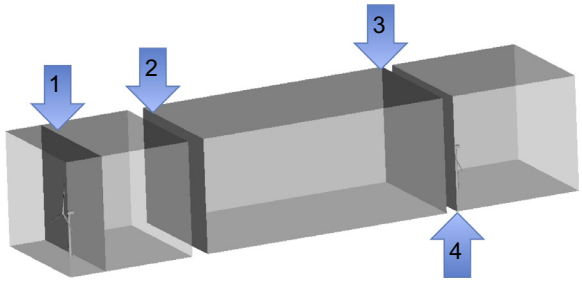

Fig. 2. Data flow between the subdomains. Velocity and temperature collected at location 1 are applied as inlet boundary conditions at location 2. Velocity and temperature collected at location 3 are applied as inlet boundary conditions at location 4. At all lateral boundaries velocity and temperature boundary conditions come from a standalone spectral/fine-difference LES.

a circular cylinder up to 300 diameters downstream [13,14], aerodynamics and FSI of a parachute crossing the far wake of an aircraft [15,16]. More recently, a spatially multiscale version of the MDM was applied to thermo-fluid analysis of a ground vehicle and its tires [17].

In the present work the MDM is employed as follows. The problem domain is divided into three subdomains (see Fig. 1 for dimensions and notation). Domains labeled *Turbine 1* and *Turbine 2* contain the upstream and downstream turbines, respectively, and domain labeled *Box* contains the space between the turbines. The three domains are simulated in a sequential manner. Velocity and temperature boundary conditions on the inflow boundary of *Turbine 1*, as well as lateral boundaries of all subdomains, are obtained from a standalone 3D LES computation of a stratified ABL with a uniform grid size of 5 m. This stratified flow computational model [103–105], which can be run in DNS or LES modes, makes use of a mixed spectral/finite-difference algorithm and the subfilter terms are handled with dynamic eddy viscosity and eddy diffusivity models. Nodal values of the velocity and temperature boundary conditions are obtained by interpolating the finite-difference solution from the structured grid of the LES simulation to the unstructured grids of the wind-turbine simulations. This data transfer strategy, employing the same dataset as in the present work, was successfully tested for the rotor-only ABL simulation in [26]. The background temperature $\bar{\phi}(x_3)$ is set to 260 K up to 100 m with an overlying inversion of strength 0.01 Km^{-1} for all domains. The geostrophic wind speed is set to 8 m/s, and the Coriolis parameter $f_c = 1.39 \times 10^{-4}$. Velocity and temperature inflow boundary conditions for *Box* are obtained using a similar data transfer strategy, where, in this case, the data is obtained by interpolating the solution on a plane positioned 10 m behind the turbine during pure aerodynamic simulation on *Turbine 1*. Inflow boundary conditions for *Turbine 2* are obtained by interpolating the solution on the outflow plane of *Box* (see Fig. 2 for details.)

Traction boundary conditions are prescribed at the outlet boundaries of all subdomains. To generate the traction values, a simulation in *Turbine 1* is performed first with the wind turbine removed, and with zero outlet traction boundary conditions. The inlet tractions produced as a result of this computation, shown in Fig. 3, are then assigned as outlet boundary conditions for all subdomains. A similar strategy was successfully employed in [26], as well as in [17] to perform a detailed thermo-fluid analysis of the rear tires of a ground vehicle.

The subdomains are discretized using triangular prisms in the boundary layer region near the wind-turbine rotors, and tetrahedra elsewhere (see Fig. 4). For *Turbine 1* and *Turbine 2* the boundary-

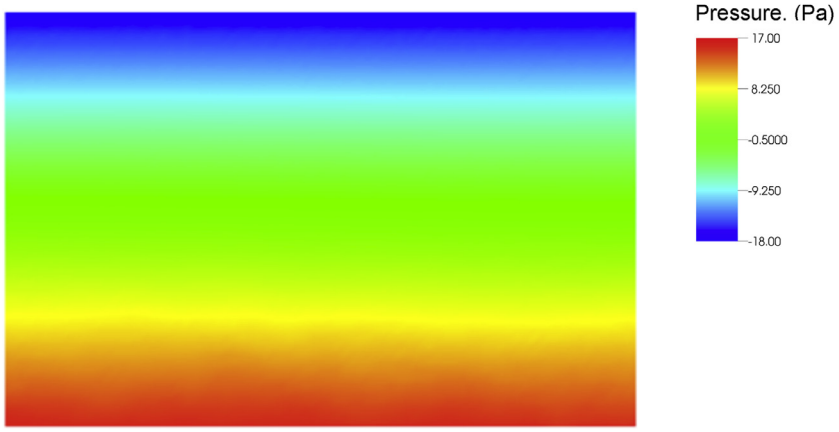

Fig. 3. Pressure profile used for outflow boundary conditions on all subdomains.

Fig. 4. Meshes employed in the wind-turbine aerodynamics and FSI simulations. Top-to-bottom: *Turbine 1*, *Box*, *Turbine 2*.

layer mesh design is based on that reported in [68]. For *Turbine 1* a total of 7,824,602 elements are used with a 4 m element length on the outer boundaries. A finer grid resolution with 2 m element length is used on a plane behind the upstream turbine where inlet data is collected for the *Box* simulation. The *Box* domain, which has a refined inner region to more accurately represent the wake turbulence, is discretized using 15,436,631 elements The *Turbine 2* domain, with a total of 9,153,426 elements, also contains a refined inner region in front of the turbine for better wake resolution.

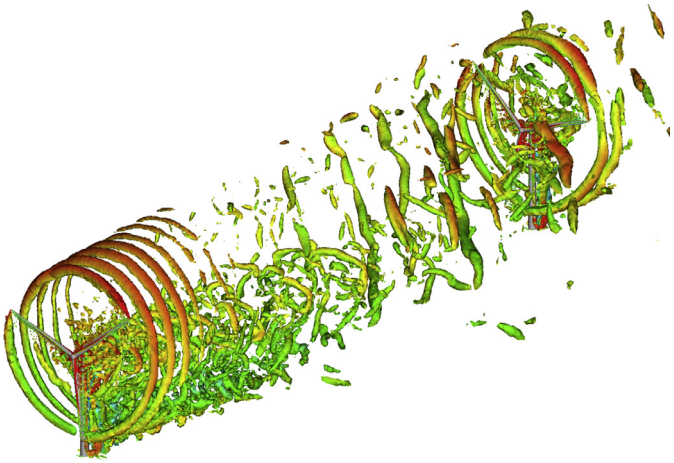

Fig. 6. 3D view of vorticity isosurfaces colored by air speed.

The time step size is set to 10^{-4} s for *Turbine 1* and *Turbine 2* simulations, and to 10^{-2} s for the *Box* simulation. The reference temperature, inversion layer height, geostrophic wind speed, and Coriolis parameter employed in the computations are all taken from [26].

4.2. Aerodynamics simulation results

Pure aerodynamics simulation results, which are also referred as "CFD", are reported in this section. During CFD simulations the wind turbine rotor is treated as a rigid, spinning object. Fig. 5 shows the velocity and temperature contours at the domain centerline. No discernible discontinuity between the subdomains is observed. A slight growth of the shear layer from the upper edge of the upstream-turbine rotor can also be seen in Fig. 5. The bottom shear layer grows much more rapidly, due to higher turbulent mixing and presence of the tower.

Fig. 6 shows vorticity isosurfaces. Rotor-tip vortices of the upstream turbine maintain a helical pattern for a distance of about one rotor diameter. They later break up, and eventually merge with vortices shed from the root and tower to form larger structures

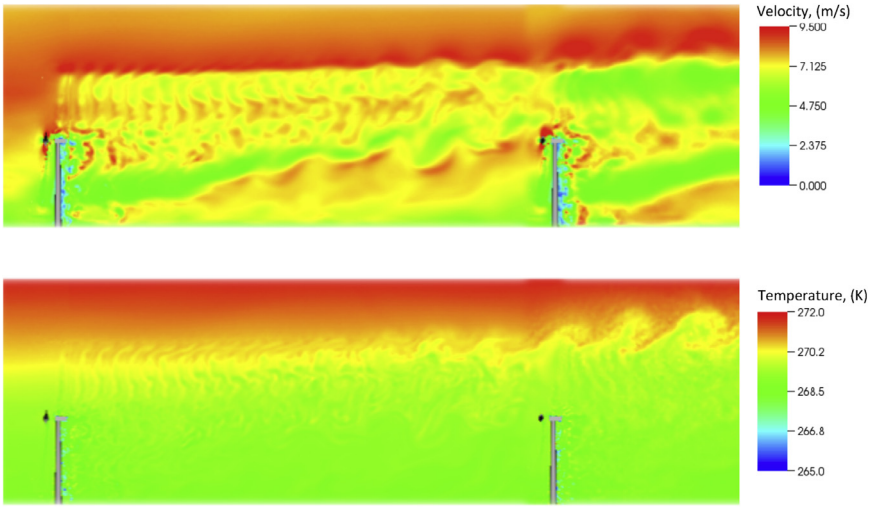

Fig. 5. 2D slice of the air speed (top) and temperature (bottom).

Fig. 7. Front view of vorticity isosurfaces colored by air speed.

at a distance between two and three rotor diameters (see Fig. 6.) These larger flow structures impact the downstream-turbine rotor and tower, and break up together with the rotor-tip vortices. The helical pattern of the rotor-tip vortices for the downstream turbine is only maintained for a short distance behind the rotor. This enhanced turbulent mixing gives a faster growth of the shear layer behind the downstream turbine.

Remark. When simulating ABL flows, the computational domain should be large enough to account for the wake drift due to side wind and Coriolis force. Fig. 7 shows the front view of the vorticity isosurfaces, where the wake drift is clearly seen. While in the present simulations wake drift is not as significant, for stronger side winds the computational domain needs to have a larger spanwise dimension.

Fig. 8 shows the air speed, averaged over six rotor revolutions, at different locations along the centerline as a function of the vertical coordinate. Air speed profile at the inlet corresponds to that imposed from the LES simulation. A short distance past *Turbine 1* the profile appears distorted, and slowly begins to recover with increasing distance from the upstream turbine. By the location of *Turbine 2* the profile begins to recover up to the hub height and above the upper-blade tip. However, qualitative differences w.r.t. the inflow profile, e.g., less near-ground shear and a higher shear above the top of the upper rotor, may be observed. In between the hub-height and upper-blade-tip locations one can clearly see the velocity deficit, which is on the order of 1–2 m/s. This velocity deficit leads to the power-production drop, as discussed in the next section.

4.3. FSI Simulation results

FSI simulations of the same multi-domain set-up are reported in this section. The wind-turbine geometry, materials, and mesh, which is comprised of 2318 quadratic NURBS shell elements, are taken from [68]. Fig. 9 shows the aerodynamic torque acting on each blade of the upstream-turbine rotor, and compares the pure aerodynamics (labeled “CFD”) and FSI results. The FSI-simulation curves exhibit low-frequency modes coming from the blade flapwise bending motions, as well as high-frequency modes coming from the blade axial torsion motions. These modes are obviously not present in the CFD curves. We note that the blade flapwise and torsional motions are not affecting the large scales of rotor-wake turbulence in a significant way. The importance of capturing these motions, which can only be done with high fidelity by solv-

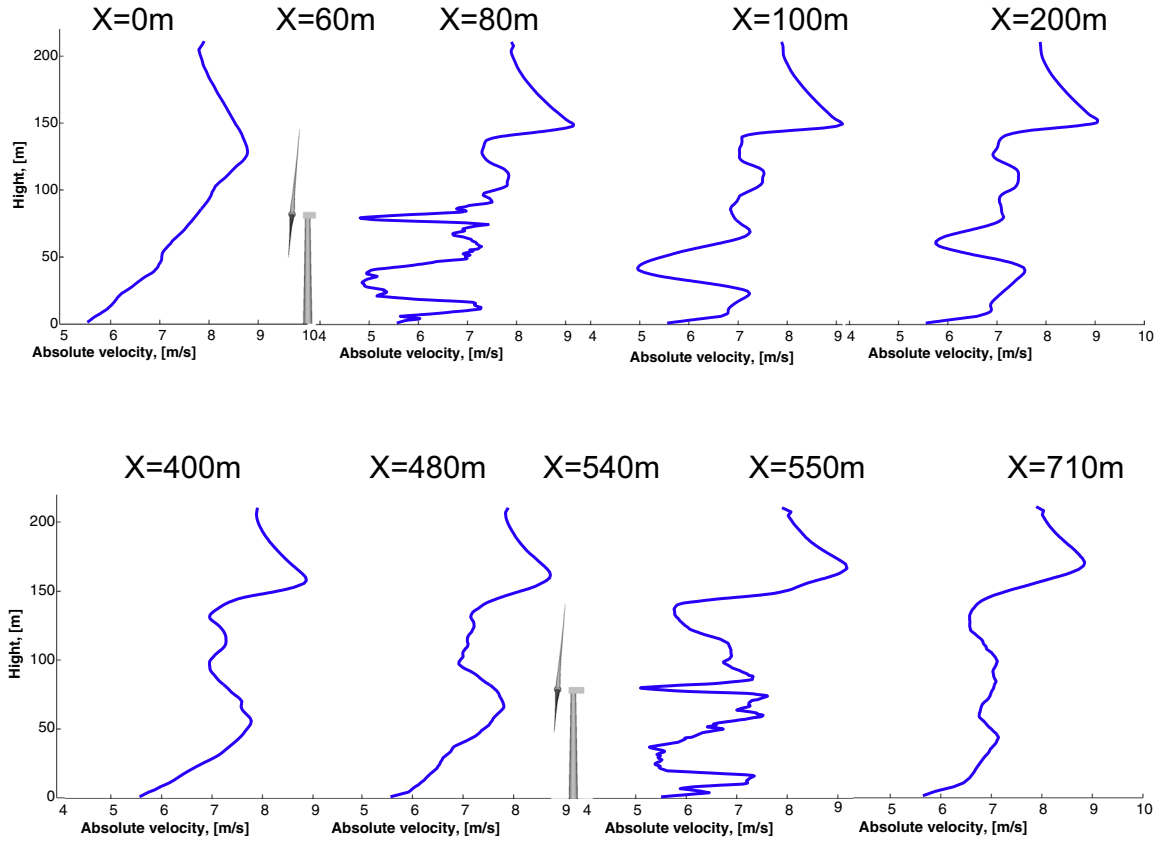

Fig. 8. Air speed averaged over six rotor revolutions and plotted at different locations along the centerline as a function of the vertical coordinate.

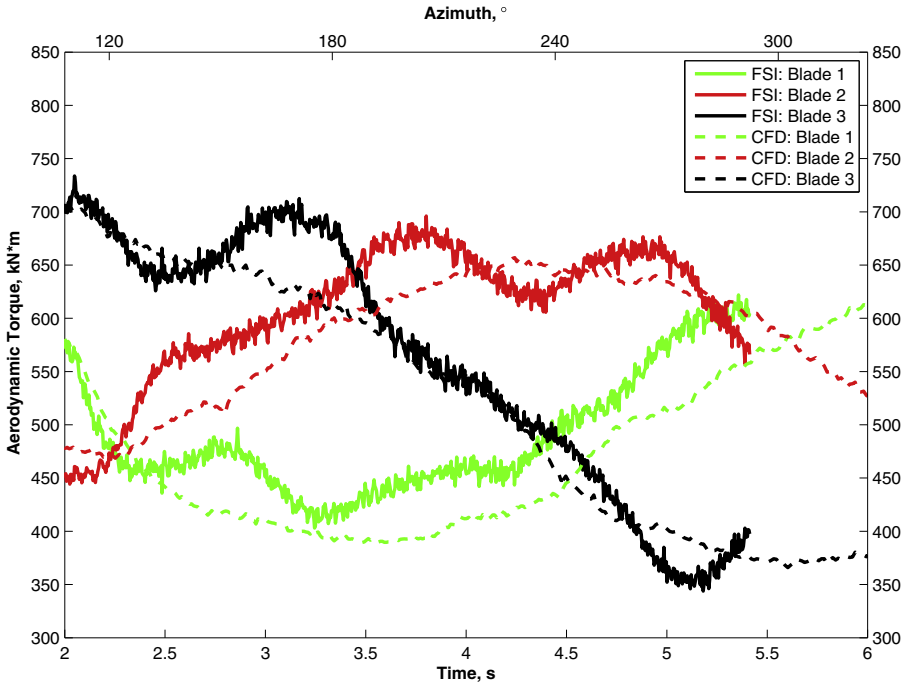

Fig. 9. Time history of the aerodynamic torque for each blade of *Turbine 1*. Comparison of pure aerodynamics (labeled "CFD") and FSI simulation results. See Fig. 1 for blade numbering.

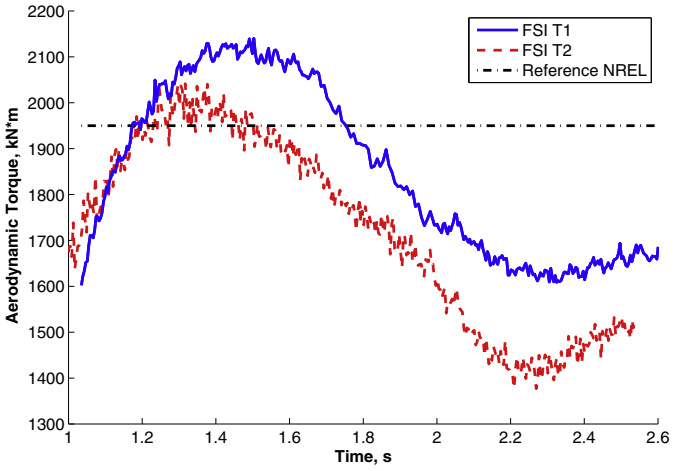

Fig. 10. Time history of the aerodynamic torque from FSI simulations for upstream (T1) and downstream (T2) turbines. Aerodynamic torque for uniform wind speed of 8 m/s from [98] is plotted for comparison.

ing a coupled FSI problem, lies in the ability to capture the blade cyclic stresses that affect the blade fatigue life (see [65].)

Fig. 10 shows a comparison of the aerodynamic torque acting on the upstream and downstream turbines. The results confirm power losses for the downstream turbine of 10–15% relative to the upstream turbine, which are due to the velocity deficit in the upstream-turbine wake. The nominal aerodynamic torque from the NREL baseline design for a uniform wind speed of 8 m/s [98] is also plotted for comparison to underscore the importance of including realistic boundary-layer flow in the aerodynamics and FSI modeling of wind turbines at full scale.

5. Conclusions

In this paper a computational FSI methodology for MDM of wind turbines is presented, and applied to the simulation of two back-to-back 5 MW wind turbines in a stably-stratified ABL. The simulations are carried out at full scale and with full complexity of wind-turbine-component geometry and material distribution. For a given set of operating conditions, a drop in power production of 10–15% between the upstream and downstream turbine is predicted by the simulation, which is within the range reported in observations by other researchers. Utilization of actual ABL conditions and strong FSI coupling were found to be important in the modeling of the blade structural response to the flow. In the future we plan to extend the current methodology to simulate multiple wind turbines arranged in arrays.

Acknowledgement

This work was supported by the NSF Award CBET-1306869 and the NSF CAREER Award. This support is gratefully acknowledged.

References

[1] Barthelmie R, Frandsen S, Rathmann O, Hansen K, Politis E, Prospathopoulos J, et al. Flow and wakes in large wind farms: final report for upwind wp8 Technical Report Report number Ris-R-1765(EN). Danmarks Tekniske Universitet, Ris Nationallaboratoriet for Bredygtig Energ; 2011.
[2] Westerhellweg A, Caadillas B, Kinder F, Neumann T. Wake measurements at alpha ventus dependency on stability and turbulence intensity. J Phys 2014;555. DOI: 10.1088/1742-6596/555/1/012106.
[3] Darema F. Dynamic data driven applications systems: a new paradigm for application simulations and measurements. In: in proceedings of ICCS 2004 4th International Conference on Computational Science; 2004. p. 662–9.
[4] Wharton S, Lundquist JK. Atmospheric stability impacts on power curves of tall wind turbines - an analysis of a west coast north american wind farm. Technical Report LLNL-TR-424425. Lawrence Livermore National Lab; 2010.
[5] Hancock P, Zhang S. A wind-tunnel simulation of the wake of a large wind turbine in a weakly unstable boundary layer. Boundary Layer Meteorol 2015;156:395–413. DOI: 10.1007/s10546-015-0037-5.
[6] Iungo G, Porte-Agel F. Volumetric lidar scanning of wind turbine wakes under convective and neutral atmospheric stability regimes. J Atmos Oceanic Technol 2014;31:2035–48.
[7] Bhaganagar K, Debnath M. Implications of stably stratified atmospheric boundary layer turbulence on the near-wake structure of wind turbines. Energies 2014;7:5740–63. doi:10.3390/en7095740.
[8] Wu Y-T, Porte-Agel F. Atmospheric turbulence effects on wind-turbine wakes: an les study. Energies 2012;5:5340–62. doi:10.3390/en5125340.

[9] Lu H, Porte-Agel F. Large-eddy simulation of a very large wind farm in a stable atmospheric boundary layer. Phys Fluids 2011;23:065101.
[10] Lee S, Churchfield M, Moriarty P, Jonkman J, Michalakes J. Atmospheric and wake turbulence impacts on wind turbine fatigue loading. Technical Report NREL/CP-5000-53567. National Renewable Energy Laboratory; 2011.
[11] Jonkman JM, Jr MLB. FAST user's guide. Tech. Rep. NREL/EL-500-38230. National Renewable Energy Laboratory, Golden, CO; 2005.
[12] Hansen K, Larsen G, Ott S. Dependence of offshore wind turbine fatigue loads on atmospheric stratification. J Phys 2014;524. doi:10.1088/1742-6596/524/1/012165.
[13] Osawa Y, Tezduyar T. A multi-domain method for 3D computation of wake flow behind a circular cylinder. Comput Fluid Dyn J 1999;8:296–308.
[14] Tezduyar T, Osawa Y. Methods for parallel computation of complex flow problems. Parallel Comput 1999;25:2039–66. doi:10.1016/S0167-8191(99)00080-0.
[15] Tezduyar T, Osawa Y. The multi-domain method for computation of the aerodynamics of a parachute crossing the far wake of an aircraft. Comput Methods Appl Mech Eng 2001;191:705–16. doi:10.1016/S0045-7825(01)00310-3.
[16] Tezduyar T, Osawa Y. Fluid–structure interactions of a parachute crossing the far wake of an aircraft. Comput Methods Appl Mech Eng 2001;191:717–26. doi:10.1016/S0045-7825(01)00311-5.
[17] Takizawa K, Tezduyar TE, Kuraishi T. Multiscale ST methods for thermo-fluid analysis of a ground vehicle and its tires. Math Models Methods Appl Sci 2015;25:2227–55. doi:10.1142/S0218202515400072.
[18] Hughes TJR, Liu WK, Zimmermann TK. Lagrangian–Eulerian finite element formulation for incompressible viscous flows. Comput Methods Appl Mech Eng 1981;29:329–49.
[19] Belytschko T, Liu WK, Moran B. Nonlinear finite elements for continua and structures. Wiley; 2000.
[20] Bazilevs Y, Takizawa K, Tezduyar TE. Computational fluid-structure interaction: methods and applications. Wiley; 2013.
[21] Bazilevs Y, Hsu M-C, Takizawa K, Tezduyar TE. ALE-VMS and ST-VMS methods for computer modeling of wind-turbine rotor aerodynamics and fluid–structure interaction. Math Models Methods Appl Sci 2012;22(supp02):1230002. doi:10.1142/S0218202512300025.
[22] Bazilevs Y, Takizawa K, Tezduyar TE. Challenges and directions in computational fluid–structure interaction. Math Models Methods Appl Sci 2013;23:215–21. doi:10.1142/S0218202513400010.
[23] Bazilevs Y, Takizawa K, Tezduyar T, Hsu M-C, Kostov N, McIntyre S. Aerodynamic and FSI analysis of wind turbines with the ALE-VMS and ST-VMS methods. Arch Comput Methods Eng 2014;21:359–98.
[24] Takizawa K, Bazilevs Y, Tezduyar TE, Long CC, Marsden AL, Schjodt K. ST and ALE-VMS methods for patient-specific cardiovascular fluid mechanics modeling. Math Models Methods Appl Sci 2014;24:2437–86.
[25] Bazilevs Y, Takizawa K, Tezduyar T. New directions and challenging computations in fluid dynamics modeling with stabilized and multiscale methods. Math Models Methods Appl Sci 2015;25:2217–26.
[26] Bazilevs Y, Korobenko A, Yan J, Pal A, Gohari S, Sarkar S. ALE–VMS Formulation for stratified turbulent incompressible flows with applications. Math Models Methods Appl Sci 2015;25(12):2349–75.
[27] Bazilevs Y, Hughes TJR. Weak imposition of dirichlet boundary conditions in fluid mechanics. Comput Fluids 2007;36:12–26.
[28] Bazilevs Y, Michler C, Calo VM, Hughes TJR. Isogeometric variational multiscale modeling of wall-bounded turbulent flows with weakly enforced boundary conditions on unstretched meshes. Comput Methods Appl Mech Eng 2010;199:780–90.
[29] Bazilevs Y, Michler C, Calo VM, Hughes TJR. Weak Dirichlet boundary conditions for wall-bounded turbulent flows. Comput Methods Appl Mech Eng 2007;196:4853–62.
[30] Golshan R, Tejada-Martínez A, Juha M, Bazilevs Y. Large-eddy simulation with near-wall modeling using weakly enforced no-slip boundary conditions. Comput Fluids 2015;118:172–81.
[31] Takizawa K, Tezduyar TE, Mochizuki H, Hattori H, Mei S, Pan L, et al. Space–time VMS method for flow computations with slip interfaces (ST-SI). Math Models Methods Appl Sci 2015;25:2377–406. doi:10.1142/S0218202515400126.
[32] Takizawa K, Tezduyar TE, Kuraishi T, Tabata S, Takagi H. Computational thermo-fluid analysis of a disk brake. Comput Mech 2016;57:965–77. doi:10.1007/s00466-016-1272-4.
[33] Bazilevs Y, Calo VM, Cottrel JA, Hughes TJR, Reali A, Scovazzi G. Variational multiscale residual-based turbulence modeling for large eddy simulation of incompressible flows. Comput Methods Appl Mech Eng 2007;197:173–201.
[34] Bazilevs Y, Akkerman I. Large eddy simulation of turbulent Taylor–Couette flow using isogeometric analysis and the residual–based variational multiscale method. J Comput Phys 2010;229:3402–14.
[35] Korobenko A, Hsu M-C, Akkerman I, Bazilevs Y. Aerodynamic simulation of vertical-axis wind turbines. J Appl Mech 2013;81(2), 021011.
[36] Hsu M-C, Akkerman I, Bazilevs Y. Wind turbine aerodynamics using ALE–VMS: validation and the role of weakly enforced boundary conditions. Comput Mech 2012;50:499–511. doi:10.1007/s00466-012-0686-x.
[37] Yan J, Augier B, Korobenko A, Czarnowski J, Ketterman G, Bazilevs Y. FSI modeling of a propulsion system based on compliant hydrofoils in a tandem configuration. Computers and Fluids 2016;141:201–11. doi:10.1016/j.compfluid.2015.07.013.
[38] Akkerman I, Dunaway J, Kvandal J, Spinks J, Bazilevs Y. Toward free-surface modeling of planing vessels: simulation of the fridsma hull using ALE-VMS. Comput Mech 2012;50:719–27.
[39] Akkerman I, Bazilevs Y, Benson DJ, Farthing MW, Kees CE. Free-surface flow and fluid–object interaction modeling with emphasis on ship hydrodynamics. J Appl Mech 2012;79:010905.
[40] Hsu M-C, Kamensky D, Bazilevs Y, Sacks MS, Hughes TJR. Fluid–structure interaction analysis of bioprosthetic heart valves: significance of arterial wall deformation. Comput Mech 2014;54:1055–71. doi:10.1007/s00466-014-1059-4.
[41] Kamensky D, Hsu M-C, Schillinger D, Evans J, Aggarwal A, Bazilevs Y, et al. An immersogeometric variational framework for fluid–structure interaction: application to bioprosthetic heart valves. Comput Methods Appl Mech Eng 2015;284:1005–53.
[42] Takizawa K, Tezduyar TE, McIntyre S, Kostov N, Kolesar R, Habluetzel C. Space–time VMS computation of wind-turbine rotor and tower aerodynamics. Comput Mech 2014;53:1–15. doi:10.1007/s00466-013-0888-x.
[43] Takizawa K. Computational engineering analysis with the new-generation space–time methods. Comput Mech 2014;54:193–211. doi:10.1007/s00466-014-0999-z.
[44] Takizawa K, Henicke B, Puntel A, Kostov N, Tezduyar TE. Computer modeling techniques for flapping-wing aerodynamics of a locust. Comput Fluids 2013;85:125–34. doi:10.1016/j.compfluid.2012.11.008.
[45] Takizawa K, Tezduyar TE, Kostov N. Sequentially-coupled space–time FSI analysis of bio-inspired flapping-wing aerodynamics of an MAV. Comput Mech 2014;54:213–33. doi:10.1007/s00466-014-0980-x.
[46] Takizawa K, Tezduyar TE, Buscher A. Space–time computational analysis of MAV flapping-wing aerodynamics with wing clapping. Comput Mech 2015;55:1131–41. doi:10.1007/s00466-014-1095-0.
[47] Takizawa K, Schjodt K, Puntel A, Kostov N, Tezduyar TE. Patient-specific computer modeling of blood flow in cerebral arteries with aneurysm and stent. Comput Mech 2012;50:675–86. doi:10.1007/s00466-012-0760-4.
[48] Takizawa K, Schjodt K, Puntel A, Kostov N, Tezduyar TE. Patient-specific computational analysis of the influence of a stent on the unsteady flow in cerebral aneurysms. Comput Mech 2013;51:1061–73. doi:10.1007/s00466-012-0790-y.
[49] Takizawa K, Tezduyar TE, Buscher A, Asada S. Space–time fluid mechanics computation of heart valve models. Comput Mech 2014;54:973–86. doi:10.1007/s00466-014-1046-9.
[50] Suito H, Takizawa K, Huynh VQH, Sze D, Ueda T. FSI analysis of the blood flow and geometrical characteristics in the thoracic aorta. Comput Mech 2014;54:1035–45. doi:10.1007/s00466-014-1017-1.
[51] Takizawa K, Montes D, McIntyre S, Tezduyar TE. Space–time VMS methods for modeling of incompressible flows at high Reynolds numbers. Math Models Methods Appl Sci 2013;23:223–48. doi:10.1142/s0218202513400022.
[52] Takizawa K, Montes D, Fritze M, McIntyre S, Boben J, Tezduyar TE. Methods for FSI modeling of spacecraft parachute dynamics and cover separation. Math Models Methods Appl Sci 2013;23:307–38. doi:10.1142/S0218202513400058.
[53] Takizawa K, Tezduyar TE, Boben J, Kostov N, Boswell C, Buscher A. Fluid–structure interaction modeling of clusters of spacecraft parachutes with modified geometric porosity. Comput Mech 2013;52:1351–64. doi:10.1007/s00466-013-0880-5.
[54] Takizawa K, Tezduyar TE, Boswell C, Kolesar R, Montel K. FSI modeling of the reefed stages and disreefing of the Orion spacecraft parachutes. Comput Mech 2014;54:1203–20. doi:10.1007/s00466-014-1052-y.
[55] Takizawa K, Tezduyar TE, Boswell C, Tsutsui Y, Montel K. Special methods for aerodynamic-moment calculations from parachute FSI modeling. Comput Mech 2015;55:1059–69. doi:10.1007/s00466-014-1074-5.
[56] Takizawa K, Tezduyar TE, Kolesar R. FSI modeling of the Orion spacecraft drogue parachutes. Comput Mech 2015;55:1167–79. doi:10.1007/s00466-014-1108-z.
[57] Yan J, Korobenko A, Tejada-Martinez A, Golshan R, Bazilevs Y. A new variational multiscale formulation for stratified incompressible turbulent flows. Comput Fluids 2016. doi:10.1016/j.compfluid.2016.12.004. Published online.
[58] Brooks AN, Hughes TJR. Streamline upwind/Petrov-Galerkin formulations for convection dominated flows with particular emphasis on the incompressible Navier–Stokes equations. Comput Methods Appl Mech Eng 1982;32:199–259.
[59] Tezduyar TE. Computation of moving boundaries and interfaces and stabilization parameters. Int J Numer Methods Fluids 2003;43:555–75. doi:10.1002/fld.505.
[60] Tezduyar T, Sathe S. Stabilization parameters in SUPG and PSPG formulations. J Comput Appl Mech 2003;4:71–88.
[61] Tezduyar TE, Sathe S. Modeling of fluid–structure interactions with the space–time finite elements: solution techniques. Int J Numer Methods Fluids 2007;54:855–900. doi:10.1002/fld.1430.
[62] Hsu M-C, Bazilevs Y, Calo VM, Tezduyar TE, Hughes TJR. Improving stability of stabilized and multiscale formulations in flow simulations at small time steps. Comput Methods Appl Mech Eng 2010;199:828–40.
[63] Hsu M-C, Bazilevs Y. Fluid–structure interaction modeling of wind turbines: simulating the full machine. Comput Mech 2012;50:821–33.
[64] Bazilevs Y, Hughes TJR. NURBS-based isogeometric analysis for the computation of flows about rotating components. Comput Mech 2008;43:143–50.
[65] Bazilevs Y, Korobenko A, Deng X, Yan J. Fluid–structure interaction modeling for fatigue-damage prediction in full-scale wind-turbine blades. J Appl Mech 2016;83(6):061010.
[66] Korobenko A, Hsu M-C, Akkerman I, Tippmann J, Bazilevs Y. Structural mechanics modeling and fsi simulation of wind turbines. Math Models Methods Appl Sci 2013;23:249–72. doi:10.1142/S0218202513400034.

[67] Bazilevs Y, Korobenko A, Deng X, Yan J, Kinzel M, Dabiri J. Fluid–structure interaction modeling of vertical-axis wind turbines. J Appl Mech 2014;81(8):081006.

[68] Bazilevs Y, Korobenko A, Deng X, Yan J. Novel structural modeling and mesh moving techniques for advanced FSI simulation of wind turbines. Int J Numer Methods Eng 2015;102:766–83. doi:10.1002/nme.4738.

[69] Kiendl J, Bletzinger K-U, Linhard J, Wüchner R. Isogeometric shell analysis with kirchhoff–love elements. Comput Methods Appl Mech Eng 2009;198:3902–14.

[70] Bazilevs Y, Hsu M-C, Kiendl J, Wüchner R, Bletzinger K-U. 3D simulation of wind turbine rotors at full scale. part II: fluid–structure interaction modeling with composite blades. Int J Numer Methods Fluids 2011;65:236–53.

[71] Kiendl J, Bazilevs Y, Hsu M-C, Wüchner R, Bletzinger K-U. The bending strip method for isogeometric analysis of Kirchhoff–Love shell structures comprised of multiple patches. Comput Methods Appl Mech Eng 2010;199:2403–16.

[72] Cottrell JA, Hughes TJR, Bazilevs Y. Isogeometric analysis: toward integration of CAD and FEA. Chichester: Wiley; 2009.

[73] Hughes TJR, Cottrell JA, Bazilevs Y. Isogeometric analysis: CAD, finite elements, NURBS, exact geometry, and mesh refinement. Comput Methods Appl Mech Eng 2005;194:4135–95.

[74] Bazilevs Y, da Veiga LB, Cottrell JA, Hughes TJR, Sangalli G. Isogeometric analysis: approximation, stability and error estimates for *h*-refined meshes. Math Models Methods Appl Sci 2006;16:1031–90.

[75] Bazilevs Y, Hsu M-C, Scott M. Isogeometric fluid–structure interaction analysis with emphasis on non-matching discretizations, and with application to wind turbines. Comput Methods Appl Mech Eng 2012;249–252:28–41.

[76] Bazilevs Y, Calo VM, Hughes TJR, Zhang Y. Isogeometric fluid–structure interaction: theory, algorithms, and computations. Comput Mech 2008;43:3–37.

[77] Chung J, Hulbert GM. A time integration algorithm for structural dynamics withimproved numerical dissipation: the generalized-α method. J Appl Mech 1993;60:371–5.

[78] Jansen K, Whiting C, Hulbert G. A generalized-α method for integrating the filtered navier–stokes equations with a stabilized finite element method. Comput Methods Appl Mech Eng 2000;190(3):305–19.

[79] Tezduyar TE. Finite element methods for flow problems with moving boundaries and interfaces. Arch Comput Methods Eng 2001;8:83–130. doi:10.1007/BF02897870.

[80] Tezduyar TE, Sathe S, Keedy R, Stein K. Space–time finite element techniques for computation of fluid–structure interactions. Comput Methods Appl Mech Eng 2006;195:2002–27. doi:10.1016/j.cma.2004.09.014.

[81] Tezduyar TE, Sathe S, Stein K. Solution techniques for the fully-discretized equations in computation of fluid–structure interactions with the space–time formulations. Comput Methods Appl Mech Eng 2006;195:5743–53. doi:10.1016/j.cma.2005.08.023.

[82] Tezduyar TE, Behr M, Mittal S, Johnson AA. Computation of unsteady incompressible flows with the finite element methods – space–time formulations, iterative strategies and massively parallel implementations. In: New Methods in Transient Analysis. PVP-Vol.246/AMD-Vol.143. New York: ASME; 1992. p. 7–24.

[83] Tezduyar T, Aliabadi S, Behr M, Johnson A, Mittal S. Parallel finite-element computation of 3D flows. Computer 1993;26(10):27–36. doi:10.1109/2.237441.

[84] Johnson AA, Tezduyar TE. Mesh update strategies in parallel finite element computations of flow problems with moving boundaries and interfaces. Comput Methods Appl Mech Eng 1994;119:73–94. doi:10.1016/0045-7825(94)00077-8.

[85] Takizawa K, Henicke B, Puntel A, Spielman T, Tezduyar TE. Space–time computational techniques for the aerodynamics of flapping wings. J Appl Mech 2012;79:010903. doi:10.1115/1.4005073.

[86] Takizawa K, Henicke B, Puntel A, Kostov N, Tezduyar TE. Space–time techniques for computational aerodynamics modeling of flapping wings of an actual locust. Comput Mech 2012;50:743–60. doi:10.1007/s00466-012-0759-x.

[87] Takizawa K, Kostov N, Puntel A, Henicke B, Tezduyar TE. Space–time computational analysis of bio-inspired flapping-wing aerodynamics of a micro aerial vehicle. Comput Mech 2012;50:761–78. doi:10.1007/s00466-012-0758-y.

[88] Tezduyar T, Aliabadi S, Behr M, Johnson A, Kalro V, Litke M. Flow simulation and high performance computing. Comput Mech 1996;18:397–412. doi:10.1007/BF00350249.

[89] Behr M, Tezduyar T. The shear-slip mesh update method. Comput Methods Appl Mech Eng 1999;174(3):261–74.

[90] Behr M, Tezduyar T. Shear-slip mesh update in 3D computation of complex flow problems with rotating mechanical components. Comput Methods Appl Mech Eng 2001;190:3189–200. doi:10.1016/S0045-7825(00)00388-1.

[91] Takizawa K, Tezduyar TE, Hattori H. Computational analysis of flow-driven string dynamics in turbomachinery. Comput Fluids 2017;142:109–17. doi:10.1016/j.compfluid.2016.02.019.

[92] Takizawa K, Tezduyar TE, Otoguro Y, Terahara T, Kuraishi T, Hattori H. Turbocharger flow computations with the space–time isogeometric analysis (ST-IGA). Comput Fluids 2017;142:15–20. doi:10.1016/j.compfluid.2016.02.021.

[93] Takizawa K, Tezduyar TE, Asada S, Kuraishi T. Space–time method for flow computations with slip interfaces and topology changes (ST-SI-TC). Comput Fluids 2016;141:124–34. doi:10.1016/j.compfluid.2016.05.006.

[94] Takizawa K, Tezduyar TE, Terahara T. Ram-air parachute structural and fluid mechanics computations with the space–time isogeometric analysis (ST-IGA). Comput Fluids 2016;141:191–200. doi:10.1016/j.compfluid.2016.05.027.

[95] Takizawa K., Tezduyar T.E., Terahara T., Sasaki T. Heart valve flow computation with the integrated Space–Time VMS, Slip Interface, Topology Change and Isogeometric Discretization methods; November 2016d. *Computers & Fluids*, published online, DOI:10.1016/j.compfluid.2016.11.012.

[96] Takizawa K, Tezduyar TE, Buscher A, Asada S. Space–time interface-tracking with topology change (ST-TC). Comput Mech 2014;54:955–71. doi:10.1007/s00466-013-0935-7.

[97] Takizawa K, Tezduyar TE. Space–time computation techniques with continuous representation in time (ST-C). Comput Mech 2014;53:91–9. doi:10.1007/s00466-013-0895-y.

[98] Jonkman J, Butterfield S, Musial W, Scott G. Definition of a 5-MW reference wind turbine for offshore system development. Technical Report NREL/TP-500-38060. National Renewable Energy Laboratory; 2009.

[99] Bazilevs Y, Hsu M-C, Akkerman I, Wright S, Takizawa K, Henicke B, et al. 3D simulation of wind turbine rotors at full scale. part I: geometry modeling and aerodynamics. Int J Numer Methods Fluids 2011;65:207–35.

[100] Takizawa K, Henicke B, Tezduyar TE, Hsu M-C, Bazilevs Y. Stabilized space–time computation of wind-turbine rotor aerodynamics. Comput Mech 2011;48:333–44.

[101] Takizawa K, Henicke B, Montes D, Tezduyar TE, Hsu M-C, Bazilevs Y. Numerical-performance studies for the stabilized space–time computation of wind–turbine rotor aerodynamics. Comput Mech 2011;48:647–57.

[102] Osawa Y, Kalro V, Tezduyar T. Multi-domain parallel computation of wake flows. Comput Methods Appl Mech Eng 1999;174:371–91. doi:10.1016/S0045-7825(98)00305-3.

[103] Gayen B, Sarkar S. Direct and large-eddy simulations of internal tide generation at a near-critical slope. J Fluid Mech 2011;681:48–79.

[104] Jalali M, Rapaka N, Sarkar S. Tidal flow over topography: effect of excursion number on wave energetics and turbulence. J Fluid Mech 2014;750:259–83.

[105] Gohari S, Sarkar S. Tidal flow over topography: effect of excursion number on wave energetics and turbulence. Boundary Layer Meteorol 2016. Accepted for publication.